Cell PRESS
Chemistry & Biology
Article

Design and Application of In Vivo FRET Biosensors to Identify Protein Prenylation and Nanoclustering Inhibitors

Monika Köhnke,[1] Steven Schmitt,[1,4] Nicholas Ariotti,[1] Andrew M. Piggott,[1] Robert G. Parton,[1,2] Ernest Lacey,[3] Robert J. Capon,[1] Kirill Alexandrov,[1,*] and Daniel Abankwa[1,5,*]
[1]Institute for Molecular Bioscience
[2]Centre for Microscopy and Microanalysis
The University of Queensland, St. Lucia, QLD 4072, Australia
[3]Microbial Screening Technologies Pty. Ltd., Building A, 28-54 Percival Road, Smithfield, NSW 2164, Australia
[4]Present address: Department of Biosystems Science and Engineering, ETH Zürich, 4058 Basel, Switzerland
[5]Present address: Turku Centre for Biotechnology, Åbo Akademi University, Turku FIN-20520, Finland
*Correspondence: k.alexandrov@uq.edu.au (K.A.), daniel.abankwa@btk.fi (D.A.)
http://dx.doi.org/10.1016/j.chembiol.2012.05.019

SUMMARY

Protein prenylation is required for membrane anchorage of small GTPases. Correct membrane targeting is essential for their biological activity. Signal output of the prenylated proto-oncogene Ras in addition critically depends on its organization into nanoscale proteolipid assemblies of the plasma membrane, so called nanoclusters. While protein prenylation is an established drug target, only a handful of nanoclustering inhibitors are known, partially due to the lack of appropriate assays to screen for such compounds. Here, we describe three cell-based high-throughput screening amenable Förster resonance energy transfer NANOclustering and Prenylation Sensors (NANOPS) that are specific for Ras, Rho, and Rab proteins. Rab-NANOPS provides the first evidence for nanoclustering of Rab proteins. Using NANOPS in a cell-based chemical screen, we now identify macrotetrolides, known ionophoric antibiotics, as submicromolar disruptors of Ras nanoclustering and MAPK signaling.

INTRODUCTION

Spatial segregation of related signaling proteins between membrane compartments is a hallmark of eukaryotic information processing. Correct membrane targeting of signaling proteins often relies on lipid modifications (Resh, 2006). Specific subcellular targeting allows lipidated proteins to execute distinct functions, through integration into spatially confined signaling networks (Groves and Kuriyan, 2010; Kholodenko et al., 2010). Three prenyltransferases, farnsesyl-transferase (FT), geranylgeranyl-transferase-1 (GGT-1), and Rab-geranylgeranyl-transferase (RabGGT) posttranslationally attach prenyl groups via a thioether linkage to C-terminal cysteines on hundreds of signaling proteins (Resh, 2006). The cysteine may be part of a recognition motif on the protein substrate, known as the CAAX box. The CAAX box (for C, cysteine; A, aliphatic residue; X, any residue), is specifically recognized by FT and/or GGT-1, depending on its exact composition (Nguyen et al., 2011; Roberts et al., 2008). In contrast, RabGGT needs an accessory protein REP for recognition of the G-domain of Rab proteins (Andres et al., 1993; Goody et al., 2005; Pylypenko et al., 2003). RabGGT transfers two geranylgeranyl moieties to two C-terminal cysteines; however, in some cases only a single cysteine is available for prenylation.

Recent studies demonstrated that the spatial distribution of several lipid-modified proteins in the membrane is not random. For instance, Ras GTPases and GPI anchored proteins form nanoclusters on the plasma membrane (Hancock, 2006; Hancock and Parton, 2005). They are highly dynamic and display lifetimes between 0.1 and 1 s. Ras nanoclusters contain only six to eight Ras molecules and are only 6–20 nm in size (Plowman et al., 2005; Prior et al., 2003). At steady state, ~40% of Ras proteins are found in nanoclusters. Importantly, isoform-specific nanoclusters produce distinct signaling outputs, thus providing another level of spatially segregated signaling. For example K-ras but not H-ras nanoclusters preferentially recruit the effector C-Raf (Plowman et al., 2008). As a result, K-ras signals stronger through this effector than H-ras (Voice et al., 1999; Yan et al., 1998). Moreover, Ras-nanoclusters act as highly sensitive signal amplifiers, thus increasing the robustness of signal transmission across the membrane (Tian et al., 2007). If nanoclustering is disrupted, signal-transduction and transforming activity of the proto-oncogene Ras are critically compromised (Paz et al., 2001; Tian et al., 2007). This confirms that nanoclustering is an indispensable feature of the Ras signaling architecture. While nanoclusters are well characterized for Ras proteins, preliminary evidence for nanoclustering of other lipidated proteins, such as of Rho proteins, Src-family kinases, and heterotrimeric G proteins exists (Abankwa and Vogel, 2007). Whether nanoclusters are also formed by small GTPases of the Rab subfamily is not known.

Clustering of these molecules was detected using Förster Resonance Energy Transfer (FRET), which is suitable to measure nanoscale proximities between fluorescently tagged molecules (Vogel et al., 2006). Computational simulations and experimental data have shown that the FRET efficiency of donor and acceptor fluorophores that are distributed randomly or partially clustered

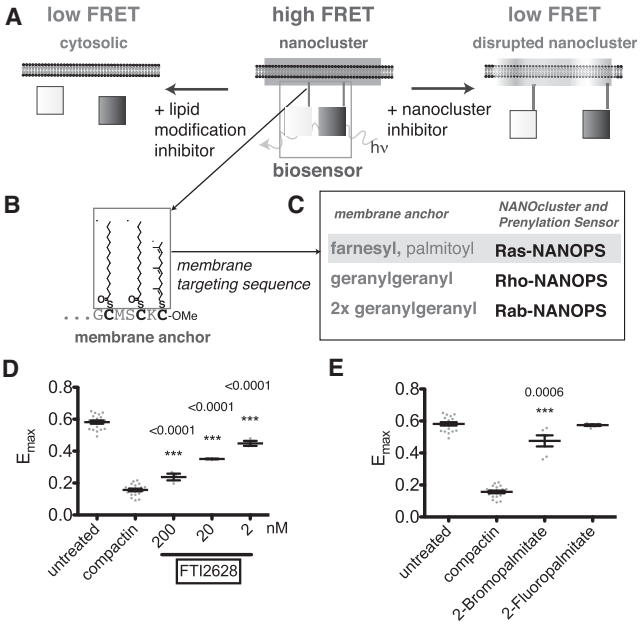

Figure 1. Nanoclustering-Based FRET Biosensors for the Detection of Lipid Transferase and Nanoclustering Inhibitors

(A and B) Schematic representation of the FRET biosensors, composed of lipid-modified membrane anchors fused to yellow and cyan fluorescent protein variants (white and gray squares, respectively).

(C) By using different membrane anchoring polypeptides, biosensors with specificity for three prenyltransferases were designed.

(D) Cytometric FRET analysis of BHK cells transfected with Ras-NANOPS and exposed to the farnesyl transferase inhibitor FTI2628 (published IC_{50}[FTI2628] = 20 nM, see Table S2) (n = 3). Response is measured as changes in the FRET value, E_{max} (Figure S7).

(E) Response of the same biosensor to 100 μM (= IC_{50}) palmitoylation inhibitors (n = 6) after 24 hr incubation. (D and E) Treatment with 5 μM compactin was used as positive control (n = 19). Individual data points (gray dots) and their mean values (horizontal black bars) with SEM are given. The number of independent experiments, n, is given above. p levels (Student's t test) are noted above the bars and in addition asterisks denote confidence levels, as explained in Experimental Procedures.

See also Figure S1.

on a membrane generally depends on the acceptor expression level and the donor-acceptor ratio (Berney and Danuser, 2003; Kiskowski and Kenworthy, 2007). Thus, FRET was applied in the recent years to study nanoclustering or nanodomain segregation of a number of proteins, such as receptors and lipid anchored proteins (Abankwa et al., 2008a; Goswami et al., 2008; Kenworthy and Edidin, 1998; Kenworthy et al., 2000; Meyer et al., 2006; Zacharias et al., 2002).

In line with their central role in extra- and intracellular signal integration, mutational activation and overexpression of membrane anchored signaling proteins have been associated with a number of diseases including cancer. One successful therapeutic approach for counteracting overactivation of such mutants is blocking their membrane anchorage through inhibition of the cognate lipid transferases. This has been successfully achieved with the development of clinically tested FT inhibitors (FTIs) and GGT-1 inhibitors (GGTIs) (Konstantinopoulos et al., 2007; Sebti and Hamilton, 2000). However, for RabGGT, as well as for myristoyl and palmitoyl transferases, only very few potent and specific inhibitors exist. This can at least partially be attributed to the lack of suitable high-throughput assays for the identification of compounds that are active in vivo. Current in vitro assays for lipid transferases suffer from high hit attrition due to poor bioavailability, high cytotoxicity, and off-target effects in the whole-cell context.

Here, we present a set of generic cell-based assays that exploit the changes in FRET arising from the dense packing of prenylated proteins into nanoclusters on their cognate membranes. Using this technology, we identified a class of natural products that inhibits nanoclustering of a H-ras-derived biosensor and affects MAPK signaling.

RESULTS

Nanoclustering-Associated FRET Reports on Functional Membrane Anchorage of Ras-Derived Probes

Although targeting protein prenylation in the context of neoplastic cellular growth has shown clinical efficacy, it inevitably has a pleiotropic effect with poorly understood consequences. As the formation of nanoclusters is critical for signaling of at least Ras oncogenes (Paz et al., 2001; Tian et al., 2007), the disruption (or prevention) of protein recruitment to nanoclusters may represent a more targeted approach of modulating cellular signaling. We therefore set out to establish, whether nanoclustering is a common feature of prenylated proteins and whether small molecules can selectively modulate it. To this end, we sought to design a generic in vivo assay to monitor nanoclustering and detect prenylation inhibitors in vivo.

We have previously shown that flow cytometric FRET measurements can detect membrane nanoclustering of lipidated proteins in mammalian cell lines (Abankwa and Vogel, 2007). In our approach, prenylatable polypeptides are genetically tagged with the fluorescent proteins mCFP or mCitrine. Both probes are coexpressed in mammalian cells, and the spontaneous organization of tagged molecules into nanoclusters is detected using FRET. We reasoned that disruption of nanoclustering, or loss of their membrane anchorage due to inhibition of their lipid modification, would lead to a concomitant reduction in FRET efficiency (Figure 1A).

Owing to its well-characterized nanoclustering properties (Abankwa et al., 2008b; Rotblat et al., 2004), we chose the extended membrane targeting sequence of the proto-oncogene H-Ras as a sensing unit to construct our first FRET biosensor, Ras-NANOcluster and Prenylation Sensor (Ras-NANOPS) (Figures 1B and 1C). The extent of nanoclustering, and therefore functional membrane anchorage, was quantified using flow cytometry, by determining the characteristic nanoclustering FRET parameter, E_{max} (Figure S7available online).

As the C terminus of H-Ras is modified by both farnesylation and palmitoylation in vivo, we expected Ras-NANOPS to report on the cellular activity of both farnesylation and palmitoylation inhibitors, as it is well documented that inhibition of prenylation also prevents subsequent palmitoylation (Hancock, 2003). We found that the biosensor dose-dependently responded to FT inhibitors such as FTI2628 (Figure 1D) and FTI277 (Figure S1A), but not to the latter's cell-impermeable prodrug form FTI276 (Figure S1B), or only weakly to inhibitors of the other

Table 1. Comparison of Nanoclustering FRET of Rab Proteins: E_{max} Values of Indicated Rab Isoforms Determined as Described in Experimental Procedures

Rab-isoform	Rab8a	Rab23	Rab5aQ79L
E_{max} ± SD (n)	26.7 ± 0.9 (5)	17.6 ± 1.8 (4)	26.0 ± 3.3 (9)

Mean values with SD and number of independent experiments (n) are given. See also Table S1.

prenyltransferases (Figures S1C and S1D). SiRNA-mediated knockdown of FT subunits also decreased FRET, however, to a lesser extent than chemical inhibition of FT (Figure S1F). We next determined, whether Ras-NANOPS could also report on the steady-state activity of palmitoyltransferases. Treatment of cells with the weak acylation inhibitors (Webb et al., 2000), 2-bromo- and 2-fluoro-palmitate for 24 hr, lead to a small change and no change in the FRET response, respectively (Figure 1E). Additional posttranslational modifications of the CAAX box, such as proteolysis and carboxymethylation, did not show a strong effect on the nanoclustering FRET (Supplemental Results, Figures S1H and S1I). These results confirmed that Ras-NANOPS could specifically and dose-dependently detect cell permeable inhibitors of farnesylated or palmitoylated membrane anchored proteins, such as H-ras.

Specific and Sensitive Detection of GGT-1 Inhibitors by Rho-NANOPS Biosensor

We expanded the concept of using nanoclustering FRET as readout for functional protein prenylation by designing a biosensor for GGT-1 geranylgeranylated Rho GTPases (Rho-NANOPS). Similar to Ras-NANOPS, we genetically fused the membrane targeting sequence of Rac1 to mCFP and mCitrine (Figure 2A). Inhibition of GGT-1 with two potent GGT-1 inhibitors led to a strong and dose-dependent decrease of E_{max} (Figure 2B and Figure S2A). Rho-NANOPS detected specific inhibition of GGT-1, as neither the specific FT inhibitor FTI2628 (Figure 2C), nor the RabGGT specific inhibitor NE10790 led to a significant response (Figure S2C). As FT and GGT-1 share a common α subunit but have specific β subunits (Seabra et al., 1991), only knockdown of the GGT-1-specific but not of the FT-specific β subunit decreased the E_{max} significantly (Figure S2D). In conclusion, Rho-NANOPS can sensitively and specifically detect inhibitors of functional membrane anchorage of Rho proteins, such as inhibitors of GGT-1.

Nanoclustering of Rab Proteins on the Plasma Membrane and on Intracellular Membranes

We next wanted to design a nanoclustering FRET biosensor for functional membrane anchorage of the third major GTPase subfamily, Rab proteins. Rabs play a key role in regulating intracellular vesicle trafficking and several Rab proteins and their lipid transferase, RabGGT itself, have been associated with the progression of cancer (Lackner et al., 2005; Stenmark, 2009).

We hypothesized that Rab proteins with Ras-like features, such as plasma-membrane targeting or mono prenylation-motif, may also nanocluster. This turned our attention to plasma membrane localized Rab8a, which contains a Ras-like CAAX prenylation motif (CSLL) (Joberty et al., 1993). We analyzed

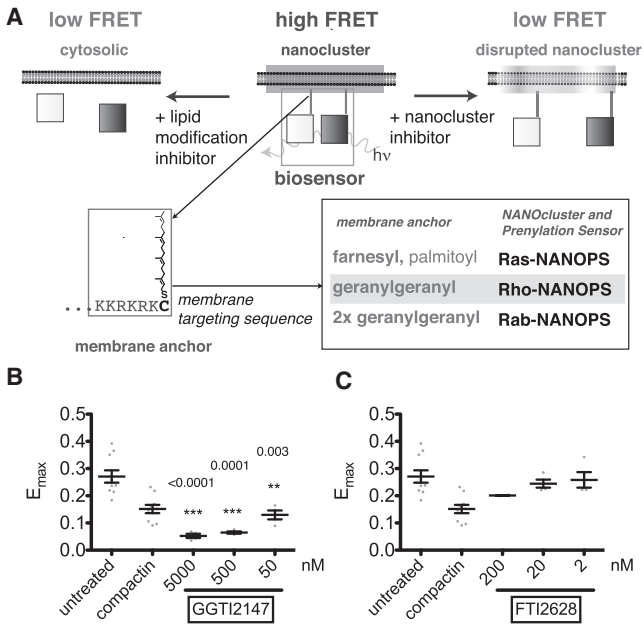

Figure 2. Rho-NANOPS Specifically Detects Cellular Steady-State Activity of GGT-1

(A) Rho-NANOPS is designed by genetic fusion of the Rac1 membrane-targeting motif to the C terminus of mCFP or mCitrine, which together form the FRET biosensor.

(B) Cytometric FRET analysis of BHK cells transfected with Rho-NANOPS and treated with a GGT-1 inhibitor, GGTI2147 (IC_{50} = 500 nM), which has >60-fold in vivo selectivity for geranylgeranylated Rap-1 over farnesylated H-ras (Vasudevan et al., 1999) (n = 4).

(C) Effect of a specific FT inhibitor FTI2628 (IC_{50} = 20 nM) as a control (n = 3). Response is measured as changes in the FRET value, E_{max}. Treatment with 5 μM compactin was used a positive control (n = 19). Individual data points (gray dots) and their mean values (horizontal black bars) with SEM are given. The number of independent experiments, n, is given above.

Statistical analysis was performed as explained in Experimental Procedures. See also Figure S2.

nanoclustering FRET of full-length Rab8a proteins that were N-terminally tagged with mCFP or mCitrine. The observed E_{max} level in the cells transfected with these constructs (Table 1) was very similar to that of Rho-NANOPS (Figure 2) and comparable to that of previous Ras-derived constructs (Abankwa et al., 2008b; Abankwa and Vogel, 2007). In order to delineate the determinants of Rab8a nanoclustering, we studied two additional Rab8a mutants. Neither introduction of an additional prenylatable cysteine on its C terminus, nor mutational activation of Rab8a, altered the E_{max} value significantly (Table S1).

Consistent with our cytometric data, FRET imaging of cells expressing Rab8a confirmed high levels of FRET on both the plasma membrane and intracellular vesicles (Figure 3A). To obtain independent evidence for Rab8a nanoclusters, we subjected plasma membrane sheets prepared from BHK cells to electron microscopic analysis. This technique, which was previously used to detect H-Ras nanoclusters (Prior et al., 2003), involves isolation of the apical plasma membrane of transfected cells grown on coverslips and immunolabeling of the exposed cytoplasmic face of the membrane. The gold labeling pattern is then analyzed in an unbiased fashion to determine the

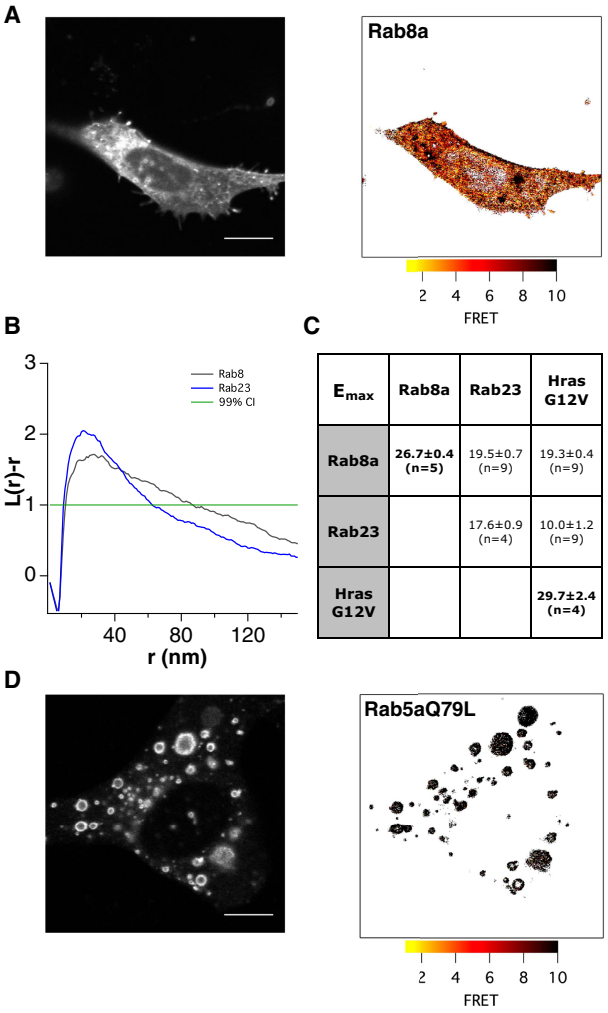

E_{max}	Rab8a	Rab23	Hras G12V
Rab8a	**26.7±0.4 (n=5)**	19.5±0.7 (n=9)	19.3±0.4 (n=9)
Rab23		17.6±0.9 (n=4)	10.0±1.2 (n=9)
Hras G12V			**29.7±2.4 (n=4)**

Figure 3. Rab Proteins Can Nanocluster on the Plasma Membrane and Intracellular Membranes

(A) Sensitizes acceptor emission FRET imaging of BHK cells coexpressing Rab8a constructs, which are N-terminally tagged with either mCFP or mCitrine. The distribution of the constructs by normal confocal imaging is shown on the left for comparison. High FRET levels are black, while absence of FRET corresponds to yellow, as indicated on the FRET-index lookup table under the FRET image (Supplemental Experimental Procedures). Scale bar is 5 μm.

(B) Electron microscopic analysis of apical membrane sheets from BHK cells expressing GFP-tagged Rab8a or Rab23. The proteins were labeled with anti-GFP antibody and visualized with 5 nm immunogold staining. Ripley's K-function analysis was performed on n = 12 plasma membrane sheets for both EGFP-Rab8a and EGFP-Rab23 (averaging 150 and 164 gold particles per 1 μm^2, respectively). Nanoclustering can be recognized as the positive deflection of the L(r)-r curve from 1, the 99% Confidence interval (CI). Maximum positive deflection of L(r)-r values above the 99% CI indicates the average cluster radius (nm).

(C) Matrix of E_{max} nanoclustering FRET values as obtained by cytometry FRET of indicated constructs that were fluorescently labeled as described in (A). Stronger nanoscale coclustering is highlighted in bold. Of note, Rab8a and Rab23 coclustering FRET is as low as that of Rab8a/H-rasG12V, suggesting that the two Rab-family proteins are in different nanodomains.

(D) FRET imaging of BHK cells expressing Rab5aQ79L-constructs, tagged as in Figure 4A. Comparison of the fluorescence intensity image (left) and the FRET image (right) shows that highly fluorescent hyperfused endosomal vesicles show high FRET levels.

Scale bars are 5 μm. See also Figure S3.

distribution of the gold particles. As can be seen in Figure 3B, this analysis confirmed that Rab8a is forming nanoclusters, where the gold label distribution has a characteristic average diameter of 27 nm. In support of our initial hypothesis, we also demonstrated by FRET- and electron microscopic-analysis nanoclustering of Rab23, which is another Rab isoform that has Ras-like features similar to Rab8a (Table 1 and Figures 3B and 3C). FRET-based coclustering analysis of cells cotransfected with both Rab8a and Rab23 indicated that these proteins populated distinct membrane nanodomains (Figure 3C) (Abankwa et al., 2008b). While Rab8a coclustered with itself with an E_{max} of 26.7 ± 0.4, the E_{max} of Rab8a and Rab23 coclustering is only 19.5 ± 0.7. Similar E_{max} differences were previously found for H- and K-ras-derived polypetides that are laterally segregated into functionally distinct nanoclusters (Abankwa et al., 2008b; Abankwa and Vogel, 2007). FRET analysis of additional Rab isoforms, Rab34 and Rab35, furthermore showed that not all predominantly plasma membrane localized Rab isoforms have high E_{max} levels (Table S1 and Figure S3A). Our data however provided conclusive evidence for Rab nanoclustering on the plasma membrane.

Next, we asked whether Rab nanoclustering occurs on internal membranes, as hinted by our Rab8a FRET imaging results. Rab5a controls endocytosis and early endosome dynamics, and is one of the best-studied Rab GTPase. When a constitutively active form of Rab5a (Rab5aQ79L) was expressed, Rab5 decorated hyperfused giant endosomes (Galperin and Sorkin, 2003; Stenmark et al., 1994) (Figure 3D). Using FRET imaging, we found that fluorescently tagged Rab5aQ79L exhibits high FRET levels on these structures (Figure 3D). Moreover, it showed a correspondingly high nanoclustering FRET E_{max} value, which was as high as that of the plasma membrane localized Rab isoforms (Table 1). This strongly suggests that Rab5a is organized into nanoclusters on internal cellular membranes.

In conclusion, we have provided evidence for the existence of Rab protein nanoclusters.

Rab-NANOPS Reports on the Steady-State Cellular Activity of RabGGT

Having demonstrated that Rab proteins can form nanoclusters, we searched systematically for a suitable Rab-construct as FRET biosensor. We determined the change in the E_{max} of 10 different Rab proteins and mutants as candidate biosensors before and after compactin treatment (Table S1). Compactin is a statin that inhibits HMG-CoA reductase in the mevalonate pathway leading to depletion of farnesyl- and geranylgeranyl pyrophosphates that serve as substrates of protein prenyltransferases. We selected Rab5aQ79L as the most suitable biosensor (hereafter, Rab-NANOPS) (Figure 4A), as it showed a high E_{max} value and a 230% decrease of E_{max} after compactin treatment (Table S1). Moreover, Rab-NANOPS showed a dose-dependent and specific FRET response to chemical inhibition of RabGGT activity by the weak but selective RabGGT inhibitor NE10790 (Figure 4C and Figures S4B–S4F). Specificity for RabGGT activity was confirmed by the significant decrease of E_{max} after RNAi-mediated ablation of RabGGT expression (Figure S4G). Using an analogous Rab8a-derived biosensor, we could also confirm that NE10790 is ineffective against monoprenylated

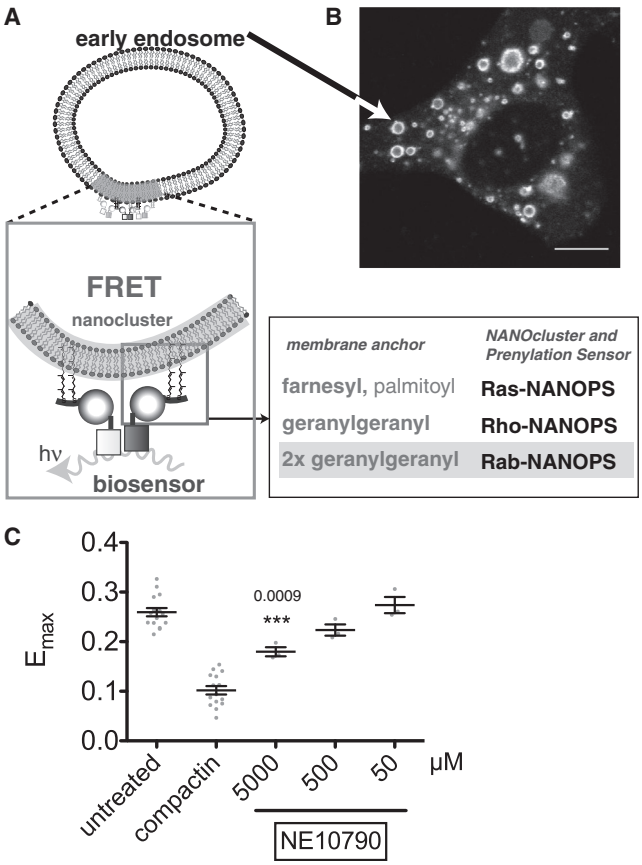

Figure 4. Rab-NANOPS Reveals Nanoclustering of Rab5aQ79L and Specifically Detects Inhibitors of Rab Prenylation

(A and B) (A) Rab-NANOPS exhibited FRET levels consistent with nanoclustering and (B) showed intense decoration of enlarged endosomal vesicles. (C) FRET in BHK cells transiently expressing this biosensor was used to detect inhibition of RabGGT by its specific inhibitor NE10790 (IC_{50} = 560 μM) (n = 3). Treatment with 5 μM compactin served as a positive control (n = 15). Individual data points (gray dots) and their mean values (horizontal black bars) with SEM are given. p levels (Student's t test) are noted above the bars and in addition asterisks denote confidence levels, as explained in Experimental Procedures. See also Figure S4.

Rab proteins in vivo (Figure S4A) (Baron et al., 2009). In summary, we have designed a FRET biosensor assay that can detect the activity of RabGGT in cells. Moreover, we have demonstrated that full-length proteins can be used as sensing unit for the steady-state activity of lipid transferases in our nanoclustering FRET-based assay.

Screening of a Natural Product Library Identifies Macrotetrolides as Ras-Nanoclustering and Ras Signaling Disrupting Agents

Due to our interest in novel inhibitors of aberrant Ras and Rab signaling, we tested whether our Ras- and Rab-NANOPS assays could be used for screening of chemical compound libraries. To evaluate the sensitivity of our assay, we measured in BHK cells the FRET response to the dose-dependent inhibition of protein prenylation by compactin in a 96-well plate format using a standard automated flow cytometer (Figures S5D–S5G and S7). Importantly, the compactin activity was detected with a sensitivity close to that obtained in HMG-CoA reductase in vitro assays (Istvan and Deisenhofer, 2001) (Figures S5D and S5E) and was >1,000 times more sensitive than the evaluation of compactin action by a cytotoxicity assay (Figure S5H). Moreover, our cytometry FRET analysis was much more efficient than the evaluation of microscopic imaging data, where in high content screening applications the subcellular relocalization is typically assessed (Figure S6A). In addition, we validated the dependence of the FRET response on the expression level and prenylation state of the biosensors by acceptor photobleaching experiments as an alternative FRET method (Figure S6B).

Next, we used the developed assay to screen a library of 540 microbial extracts selected from a larger extract collection with over 400,000 members optimized for chemical and structural diversity. Using a 20% reduction of the characteristic E_{max} as hit criterion in our screen we conducted primary and secondary screens and confirmed 19 and 18 extracts with promising Ras- and Rab-NANOPS responses, respectively. The responses in four extracts were shared by both biosensors, while the majority of active extracts exerted biosensor-specific effects. These results suggest the existence of selective as well as broad-spectrum actives (Figure 5A). In follow-up experiments, we focused on eight extracts, which showed overlapping and/or strong activity for Ras- and Rab-NANOPS. For several of these extracts, the activity was enriched in the most hydrophobic fractions following reversed phase chromatography (Figures S8A and S8B).

Analysis of the metabolite profiles of the selected hits revealed that five out of eight extracts contained macrotetrolides, which are macrocyclic antibiotics known for their ionophoric activity (Figure 5B) (Graven et al., 1966). Using a mixture of macrotetrolides (nonactin, monactin, dinactin, trinactin and tetranactin) in our cellular FRET assay, we first validated their dose-dependent action on the E_{max} response of Ras-NANOPS (Figure 5C). The IC_{50} of 1.9 μg/ml suggested that macrotetrolides are active in the low micromolar range. We next tested, whether macrotetrolides can act synergistically to classical inhibitors of protein prenylation. Indeed, our analysis of the FRET response confirmed that macrotetrolides act in concert with compactin and FTIs, shifting the apparent IC_{50} down by a factor of two to five (Figure 5D; Figure S8C).

As ionophores, macrotetrolides can insert into the cellular membranes. This may impact on the membrane nanostructure, possibly disrupting nanoclusters harboring small GTPases. To test this hypothesis, we performed electron microscopic analysis of Ras-biosensor nanoclustering on plasma membrane-derived membrane sheets (Prior et al., 2003). As can be seen in Figure 5E, the macrotetrolides induced a significant and specific reduction in nanoclustering of the Ras-biosensor construct (Figures S9A and S9B). This reduction was as high as that mediated by the cholesterol-extracting agent methyl-β-cyclodextrin (MbCD), which is known to disperse Ras nanoclusters (Prior et al., 2003).

The ionophoric activity may have altered the cellular membrane potential and thus affect membrane localization in particular of K-ras4B (Gomez and Daniotti, 2007). However, this was not evidenced by confocal imaging data, which showed that neither subcellular localization of Ras-NANOPS,

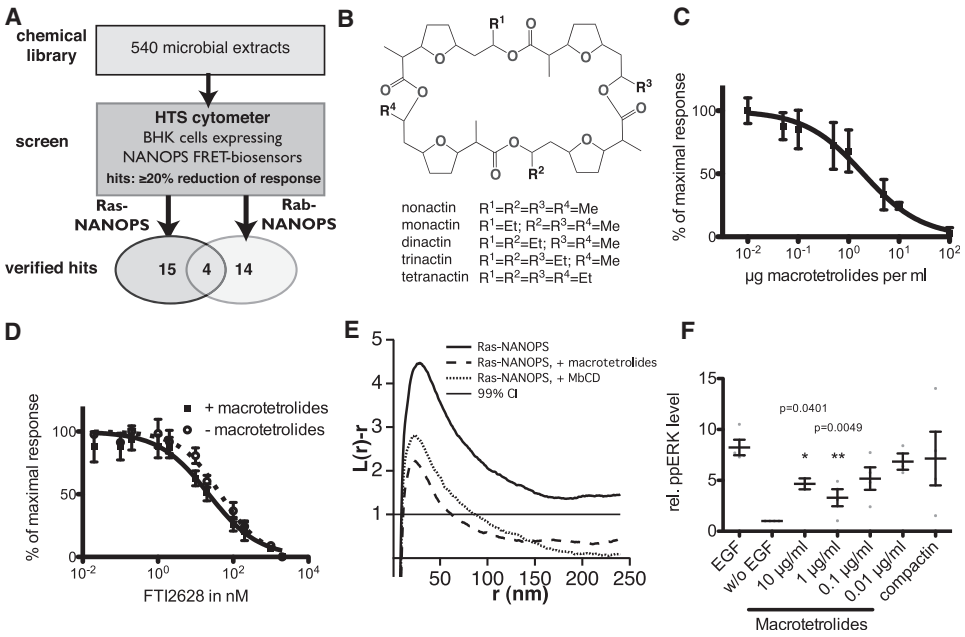

Figure 5. Screening of a Natural Product Library with Ras- and Rab-NANOPS Identifies Macrotetrolides as Ras Nanoclustering and Ras Signaling Disrupting Compounds

(A) Schematic overview of the flow cytometeric 96-well-based high-throughput screen (HTS) of a library of microbial extracts. The number of verified hits per biosensor is shown in a Venn diagram.

(B) Chemical structure of macrotetrolides.

(C) Dose-response curve of the effect of the mixture of macrotetrolides on the nanoclustering E_{max} value of Ras-NANOPS expressed in BHK cells (n = 3), IC_{50} = 1.9 µg/ml.

(D) Two Ras-NANOPS FRET dose-response curves of FTI2628 are shown, with (+ macrotetrolides, 10 µg/ml, solid curve, n = 3, IC_{50} = 22.3 nM) and without macrotetrolides (– macrotetrolides, dotted curve, n = 3 IC_{50} = 45.6 nM).

(E) Apical membrane sheets from BHK cells expressing Ras-NANOPS were generated, immunogold labeled with 5 nm anti-GFP antibody and imaged by electron microscopy. Ripley's K-function and bootstrap analyses were performed after indicated treatments (untreated, macrotetrolides for 24 hr, methyl-beta-cyclodextrin, MbCD for 1 hr, on n = 16, n = 16 and n = 10 plasma membrane sheets, respectively). Macrotetrolide treatment resulted in a significant decrease in nanoclustering (p = 0.012) of Ras-NANOPS, whereas, MbCD treatment did not result in a significant decrease (p = 0.42). Average numbers of gold particles per 1 μm^2 were consistent between experimental conditions (untreated = 1,023, macrotetrolides = 1,006 and MbCD = 1,229).

(F) EGF-stimulated MAPK response of BHK cells measured by changes in levels of ERK phosphorylation (n ≥ 3, except for 10 µg/ml where n = 2). Cells were treated for 24 hr with the indicated inhibitors. Compactin was applied at 5 µM. Individual data points (gray dots) and their mean values (horizontal black bars) with SEM are given in (C), (D), and (F). Statistical analysis in (F) was as described in Figure 1.

See also Figures S5, S6, S7, S8, S9, and S10.

nor mGFP-H-ras, nor mGFP-K-ras4B (Figure S10) were significantly affected by macrotetrolides.

To test for more subtle effects of the ionophoric activity on K-ras nanoclustering, we analyzed the effect of macrotetrolides on the E_{max} of Rho-NANOPS, which contains a polybasic membrane anchoring C terminus similar to K-ras, or an analogous K-ras-derived biosensor (Abankwa and Vogel, 2007) (Figures S9F and S9G). Neither the nanoclustering FRET of Rho-NANOPS, nor that of the K-ras-derived biosensor was affected by macrotetrolides. Finally, biochemical experiments confirmed that overall protein prenylation by farnesyltransferase or Rab-geranylgeranlytransferase was unaffected by macrotetrolides (Figures S9D and S9E). In summary, these data suggest that macrotetrolides specifically disrupt nanoclustering of Ras-NANOPS, while membrane localization of H- and K-ras, as well as protein prenylation, remains unaffected.

Ras nanoclustering is essential for its signal transmission in the MAPK pathway (Tian et al., 2007). We therefore examined the biological effect of macrotetrolides on Ras/MAPK signaling activity. In agreement with the importance of Ras nanoclustering for Ras signaling, incubation of BHK cells with macrotetrolides decreased the epidermal growth factor(EGF)-induced ppERK levels dose dependently (Figure 5F). Finally, to get more information about individual active compounds, we fractionated the macrotetrolide mix by reversed phase HPLC. The nanocluster-dispersing activity was detected in several fractions, including one containing nonactin and monactin. In fact, the mixture of these two macrotetrolides could dose-dependently decrease the FRET response with a submicromolar IC_{50} of approximately 0.32 µM (Figure S9C), which corresponds to a higher activity than that found for the macrotetrolide mix (Figure 5C).

In conclusion, using our cellular FRET screen, we have identified macrotetrolides as submicromolar inhibitors of Ras membrane nanoclustering. With this mode of action, they can act synergistically with classical inhibitors, such as compactin and FTIs, to inhibit functional membrane anchorage of Ras. Most importantly, this activity is sufficient to significantly

decrease Ras/MAPK signaling, which is often aberrantly upregulated in cancer.

DISCUSSION

We have developed a sensitive high-throughput assay for in vivo monitoring of the steady-state activity of all three eukaryotic prenyl-transferases that previously could only be analyzed in vitro. This direct and quantitative assessment of the inhibition of selected molecular drug targets in the environment of intracellular membranes sets this assay apart from previous developments. Furthermore, we have demonstrated that the FRET assay can be used to evaluate such complex sources of bioactive compounds as microbial extracts. This highlights the robustness, stability, and selectivity of the bioassay and its relevance to the in vivo situation.

We anticipate that the analysis of membrane anchorage by FRET can be used for related applications, such as deorphanization of the in vivo targets of palmitoyltransferases. This can be achieved by simple customization of the system, as essentially any nanoclustered polypeptide can be redesigned into a biosensor.

Our analysis also provides direct evidence of clustering of Rab GTPases on the nanoscale. The different extent of nanoclustering FRET of Rab5a mutants suggests that Rab5a needs a specific proteolipid environment on endosomes for nanocluster formation. This is consistent with the specific set of endosomal proteins, such as guanine nucleotide exchange factors (GEFs) and effectors, that were proposed to reinforce Rab5 clustering (Zerial and McBride, 2001). While the FRET data analysis is necessarily performed at overexpression levels, we have shown previously (Abankwa and Vogel, 2007), that high FRET levels that are consistent with nanoclustering are already achieved at physiological densities of 50–200 proteins per μm^2 (Gureasko et al., 2008). Our Rab nanoclustering FRET data are further supported by our electron microscopic analysis and the coclustering analysis with Ras as a well-established nanoclustered protein. Considering the importance of nanoclustering for Ras signal transmission and Ras activation (Gureasko et al., 2008; Tian et al., 2007), and the now suggested significance for the signaling architecture at least of a subset of small GTPases, nanoclusters may represent putative drug targets.

Most importantly, we have identified macrotetrolides as submicromolar Ras-NANOPS nanoclustering inhibitors. While the identified compound class has been known to possess antibiotic activity for many decades (Graven et al., 1966), their potential to inhibit Ras nanoclustering and MAPK signaling has only become apparent through our FRET biosensor assay. The nanocluster disrupting activity does warrant further development of the structure class and prompts a closer analysis of other lipophylic ionophores.

SIGNIFICANCE

Despite three decades of efforts, no specific inhibitor of the oncoprotein Ras has been developed. While chemical screening typically relies on biochemical assays, recent data have emphasized the importance of the membrane environment of the intact cell for Ras functionality. Membrane nanoclustering of Ras molecules is necessary for their biological activity. Different Ras isoforms laterally segregate to different nanoclusters from where they appear to engage signaling pathways specifically. It is therefore tempting to speculate that Ras nanoclusters may represent novel, specific anti-Ras drug targets.

To test this idea, we developed three nanocluster FRET biosensors with the potential to identify classical membrane targeting inhibitors (e.g., FTIs, statins) and nanoclustering inhibitors of the three major subfamilies of Ras, Rho, and Rab GTPases.

Our results show that by using a FRET-based high-throughput cytometric assay it was possible to identify specific submicromolar inhibitors of Ras nanoclustering that also block MAPK signaling. We also provide evidence that Rab-GTPases are nanoclustered, suggesting that targeting small GTPase nanoclusters could be a novel, generic approach to block small GTPase signaling. Rab proteins and their cognate prenyltransferase are recently identified cancer-drug targets, and our assay represents a cellular assay that can identify the corresponding inhibitors. This relatively simple and high-throughput amenable assay has therefore potential for cellular screening of not only mixed but also defined chemical libraries. Finally, our biosensor approach could be extended to probe the cellular activity of other protein lipid transferases.

EXPERIMENTAL PROCEDURES

Cell Culture

BHK 21 cells (Sigma-Aldrich) were cultured in Dulbecco's modified Eagle's medium (DMEM, Invitrogen) supplemented with 10% fetal bovine serum, 100 U/ml penicillin G, (Invitrogen, # 15070-063), and 100 U/ml streptomycin (Invitrogen, #15070-063). HEK293 cells (Sigma-Aldrich) were cultured in DMEM containing 10% fetal bovine serum (Invitrogen, #26140079), 1% glutamine (Invitrogen, #25030-081), 1% nonessential amino acids (Invitrogen, #11140050), 100 U/ml penicillin G and 100 U/ml streptomycin and incubated at 37°C with 5% CO_2. Transfections were performed with FuGene6 (Roche) according to the manufacturer's instructions in a 6-well plate and the cells transferred to a 96-well plate on the next day with a density of 5×10^4 cells per well. The compound stocks were dissolved in DMSO (Sigma Aldrich, #41641) (all, but compactin and NE10790, which were dissolved in water) and diluted in cell culture medium for experiments to give a final DMSO concentration below 0.3%. All inhibitors (Table S2) were added to cultured cells 16 hr after transfection and cultures were incubated for 24 hr. A list of reagents is provided in the supporting information to this manuscript. The pilot screening of the 540 bacterial extracts from Microbial Screening Technologies Pty. Ltd. (MST), which represents a large cross-section of chemical diversity, was performed similarly by diluting the extracts 1:10 in 100 μl cell-assay in a 96-well plate and incubating them for 24 hr.

Flow Cytometric FRET Analysis

For flow cytometric analysis, cells were detached with 10 mM EDTA in PBS and fixed in 2% paraformaldehyde (final concentration). The measurements were performed on a FACS CantoII (BD biosciences) equipped with a high-throughput sampler, using the following filters for donor (405 nm excitation, 450/50 nm emission filter), acceptor (488 nm, excitation, 585/42 nm emission filter), and FRET channel (488 nm excitation, 530/30 nm emission filter). The flow cytometer data were analyzed for FRET with a custom written procedure in IgorPro5 (Wavemetrics), as described (Abankwa et al., 2008b; Abankwa and Vogel, 2007). In brief, doublet discrimination was implemented to measure signals of single cells. For normalized acceptor level calibration, cA, FITC beads (Bangs Laboratories) with a defined size and fluorescein content were used as described previously. A mCFP-mCitrine fusion protein was used to

calibrate for the FRET efficiency and donor-acceptor ratio. Only cells with a donor mole-fraction, $x_D = 0.5 \pm 0.1$ were analyzed. The E_{max} value was determined as described (Abankwa et al., 2008b; Abankwa and Vogel, 2007).

Electron Microscopy and Statistical Analyses

Plasma membrane sheets were generated from BHK cells, fixed with 4% paraformaldehyde and 0.1% glutaraldehyde and labeled with anti-GFP antibody directly conjugated to 5 nm colloidal gold as described previously (Plowman et al., 2005; Prior et al., 2003). Electron micrographs of labeled PM sheets were imaged at 80 kV in a JEOL 1011 transmission electron microscope (JEOL, Japan) at a magnification of 100,000 times. xy coordinates of gold particles were determined using ImageJ (Hancock and Prior, 2005; Prior et al., 2003) and Ripley's K function statistical analysis was performed on xy coordinates as described previously (Plowman et al., 2005; Prior and Hancock, 2001). Bootstrap tests were employed to compare differences between point patterns and were performed as described previously (Diggle et al., 2000).

siRNA Knockdown Experiments and RT-PCR Quantification

HEK293 were seeded in a 12-well plate and siRNA transfection was performed on the next day with Lipofectamine RNAiMax (Invitrogen) according to the manufacturer's instructions with a final concentration of 40 nM siRNA in the medium. Cells were harvested 48 hr after transfection, and RNA extraction and cDNA synthesis (CellSure, Bioline) were performed according to the manufacturer's protocol. The real-time PCR consisted of cDNA template (diluted 1:20), forward and reverse primers (200 nM final concentration), and Platinum SYBR Green qPCR Supermix-UDG (Invitrogen) in a total volume of 20 μl. Glyceraldehyde 3-phosphate dehydrogenase (GAPDH) was used as normalization reference. Quantitative real-time PCR was carried out in triplicate on indicated number of independent templates on a 7500 Real-Time PCR System (Applied Biosystems). For analysis of the Ct values, the ΔΔCt method was applied. To test for contamination, standard control PCRs were performed. For FACS analysis of the knockdown, DNA transfection of the biosensor constructs with FuGene6 was performed 24 hr after siRNA transfection. The cells were analyzed for FRET on the flow cytometer as described above, 48 hr after siRNA transfection. Employed siRNAs are provided in Table S3.

Data Analysis

The IC_{50} values for inhibition data were analyzed in GraphPad Prism by nonlinear regression analysis on log (inhibitor) versus (normalized) response data using the Marquardt method.

Statistical Analysis

Z′ scores were calculated on the control data in the chemical screen from the following formula $Z' = 1 - (3 \cdot \sigma_{pos} + 3 \cdot \sigma_{neg})/(|\mu_{pos} - \mu_{neg}|)$, with $\sigma_{pos/neg}$: SDs of positive and negative controls, respectively, and $\mu_{pos/neg}$: averages of positive and negative controls, respectively (Zhang et al., 1999). Significant differences between mean values of inhibitor treated samples and mean values of untreated samples were analyzed using two-tailed Student's t tests in GraphPad Prism or Microsoft Excel. Confidence p levels are given and in addition indicated by asterisks, with *$p < 0.05$, **$p < 0.01$, and ***$p < 0.001$. Note, that "untreated" and "compactin"-treated samples were always significantly different ($p < 0.001$). Therefore, for clarity these p levels are not shown.

SUPPLEMENTAL INFORMATION

Supplemental Information includes eleven figures, three tables, Supplemental Results, Supplemental Discussion, and Supplemental Experimental Procedures and can be found with this article online at http://dx.doi.org/10.1016/j.chembiol.2012.05.019.

ACKNOWLEDGMENTS

This work was supported in part by NHMRC Grants 569652 and 511003 (Australia), ARC Grants DP1094080 and LP0989954 (Australia), and Cancer Australia Grant 631471. Confocal imaging was supported by the facilities of the Australian Cancer Research Foundation (ACRF). We thank Veronika Schreiber for technical help.

Received: January 22, 2012
Revised: May 25, 2012
Accepted: May 30, 2012
Published: July 26, 2012

REFERENCES

Abankwa, D., and Vogel, H. (2007). A FRET map of membrane anchors suggests distinct microdomains of heterotrimeric G proteins. J. Cell Sci. *120*, 2953–2962.

Abankwa, D., Gorfe, A.A., and Hancock, J.F. (2008a). Mechanisms of Ras membrane organization and signalling: Ras on a rocker. Cell Cycle *7*, 2667–2673.

Abankwa, D., Hanzal-Bayer, M., Ariotti, N., Plowman, S.J., Gorfe, A.A., Parton, R.G., McCammon, J.A., and Hancock, J.F. (2008b). A novel switch region regulates H-ras membrane orientation and signal output. EMBO J. *27*, 727–735.

Andres, D.A., Seabra, M.C., Brown, M.S., Armstrong, S.A., Smeland, T.E., Cremers, F.P., and Goldstein, J.L. (1993). cDNA cloning of component A of Rab geranylgeranyl transferase and demonstration of its role as a Rab escort protein. Cell *73*, 1091–1099.

Baron, R.A., Tavaré, R., Figueiredo, A.C., Błazewska, K.M., Kashemirov, B.A., McKenna, C.E., Ebetino, F.H., Taylor, A., Rogers, M.J., Coxon, F.P., and Seabra, M.C. (2009). Phosphonocarboxylates inhibit the second geranylgeranyl addition by Rab geranylgeranyl transferase. J. Biol. Chem. *284*, 6861–6868.

Berney, C., and Danuser, G. (2003). FRET or no FRET: a quantitative comparison. Biophys. J. *84*, 3992–4010.

Diggle, P.J., Mateu, J., and Clough, H.E. (2000). A comparison between parametric and non-parametric approaches to the analysis of replicated spatial point patterns. Adv. Appl. Probab. *32*, 331–343.

Galperin, E., and Sorkin, A. (2003). Visualization of Rab5 activity in living cells by FRET microscopy and influence of plasma-membrane-targeted Rab5 on clathrin-dependent endocytosis. J. Cell Sci. *116*, 4799–4810.

Gomez, G.A., and Daniotti, J.L. (2007). Electrical properties of plasma membrane modulate subcellular distribution of K-Ras. FEBS J. *274*, 2210–2228.

Goody, R.S., Rak, A., and Alexandrov, K. (2005). The structural and mechanistic basis for recycling of Rab proteins between membrane compartments. Cell. Mol. Life Sci. *62*, 1657–1670.

Goswami, D., Gowrishankar, K., Bilgrami, S., Ghosh, S., Raghupathy, R., Chadda, R., Vishwakarma, R., Rao, M., and Mayor, S. (2008). Nanoclusters of GPI-anchored proteins are formed by cortical actin-driven activity. Cell *135*, 1085–1097.

Graven, S.N., Lardy, H.A., Johnson, D., and Rutter, A. (1966). Antibiotics as tools for metabolic studies. V. Effect of nonactin, monactin, dinactin, and trinactin on oxidative phosphorylation and adenosine triphosphatase induction. Biochemistry *5*, 1729–1735.

Groves, J.T., and Kuriyan, J. (2010). Molecular mechanisms in signal transduction at the membrane. Nat. Struct. Mol. Biol. *17*, 659–665.

Gureasko, J., Galush, W.J., Boykevisch, S., Sondermann, H., Bar-Sagi, D., Groves, J.T., and Kuriyan, J. (2008). Membrane-dependent signal integration by the Ras activator Son of sevenless. Nat. Struct. Mol. Biol. *15*, 452–461.

Hancock, J.F. (2003). Ras proteins: different signals from different locations. Nat. Rev. Mol. Cell Biol. *4*, 373–384.

Hancock, J.F. (2006). Lipid rafts: contentious only from simplistic standpoints. Nat. Rev. Mol. Cell Biol. *7*, 456–462.

Hancock, J.F., and Parton, R.G. (2005). Ras plasma membrane signalling platforms. Biochem. J. *389*, 1–11.

Hancock, J.F., and Prior, I.A. (2005). Electron microscopic imaging of Ras signaling domains. Methods *37*, 165–172.

Istvan, E.S., and Deisenhofer, J. (2001). Structural mechanism for statin inhibition of HMG-CoA reductase. Science *292*, 1160–1164.

Joberty, G., Tavitian, A., and Zahraoui, A. (1993). Isoprenylation of Rab proteins possessing a C-terminal CaaX motif. FEBS Lett. *330*, 323–328.

Kenworthy, A.K., and Edidin, M. (1998). Distribution of a glycosylphosphatidylinositol-anchored protein at the apical surface of MDCK cells examined at a resolution of <100 A using imaging fluorescence resonance energy transfer. J. Cell Biol. *142*, 69–84.

Kenworthy, A.K., Petranova, N., and Edidin, M. (2000). High-resolution FRET microscopy of cholera toxin B-subunit and GPI-anchored proteins in cell plasma membranes. Mol. Biol. Cell *11*, 1645–1655.

Kholodenko, B.N., Hancock, J.F., and Kolch, W. (2010). Signalling ballet in space and time. Nat. Rev. Mol. Cell Biol. *11*, 414–426.

Kiskowski, M.A., and Kenworthy, A.K. (2007). In silico characterization of resonance energy transfer for disk-shaped membrane domains. Biophys. J. *92*, 3040–3051.

Konstantinopoulos, P.A., Karamouzis, M.V., and Papavassiliou, A.G. (2007). Post-translational modifications and regulation of the RAS superfamily of GTPases as anticancer targets. Nat. Rev. Drug Discov. *6*, 541–555.

Lackner, M.R., Kindt, R.M., Carroll, P.M., Brown, K., Cancilla, M.R., Chen, C., de Silva, H., Franke, Y., Guan, B., Heuer, T., et al. (2005). Chemical genetics identifies Rab geranylgeranyl transferase as an apoptotic target of farnesyl transferase inhibitors. Cancer Cell *7*, 325–336.

Meyer, B.H., Segura, J.M., Martinez, K.L., Hovius, R., George, N., Johnsson, K., and Vogel, H. (2006). FRET imaging reveals that functional neurokinin-1 receptors are monomeric and reside in membrane microdomains of live cells. Proc. Natl. Acad. Sci. USA *103*, 2138–2143.

Nguyen, U.T., Goodall, A., Alexandrov, K., and Abankwa, D. (2011). Isoprenoid modifications. In Post-Translational Modifications in Health and Disease, C.J. Vidal, ed. (New York: Springer), p. 486.

Paz, A., Haklai, R., Elad-Sfadia, G., Ballan, E., and Kloog, Y. (2001). Galectin-1 binds oncogenic H-Ras to mediate Ras membrane anchorage and cell transformation. Oncogene *20*, 7486–7493.

Plowman, S.J., Muncke, C., Parton, R.G., and Hancock, J.F. (2005). H-ras, K-ras, and inner plasma membrane raft proteins operate in nanoclusters with differential dependence on the actin cytoskeleton. Proc. Natl. Acad. Sci. USA *102*, 15500–15505.

Plowman, S.J., Ariotti, N., Goodall, A., Parton, R.G., and Hancock, J.F. (2008). Electrostatic interactions positively regulate K-Ras nanocluster formation and function. Mol. Cell. Biol. *28*, 4377–4385.

Prior, I.A., and Hancock, J.F. (2001). Compartmentalization of Ras proteins. J. Cell Sci. *114*, 1603–1608.

Prior, I.A., Muncke, C., Parton, R.G., and Hancock, J.F. (2003). Direct visualization of Ras proteins in spatially distinct cell surface microdomains. J. Cell Biol. *160*, 165–170.

Pylypenko, O., Rak, A., Reents, R., Niculae, A., Sidorovitch, V., Cioaca, M.D., Bessolitsyna, E., Thomä, N.H., Waldmann, H., Schlichting, I., et al. (2003). Structure of Rab escort protein-1 in complex with Rab geranylgeranyltransferase. Mol. Cell *11*, 483–494.

Resh, M.D. (2006). Palmitoylation of ligands, receptors, and intracellular signaling molecules. Sci. STKE *2006*, re14.

Roberts, P.J., Mitin, N., Keller, P.J., Chenette, E.J., Madigan, J.P., Currin, R.O., Cox, A.D., Wilson, O., Kirschmeier, P., and Der, C.J. (2008). Rho Family GTPase modification and dependence on CAAX motif-signaled posttranslational modification. J. Biol. Chem. *283*, 25150–25163.

Rotblat, B., Prior, I.A., Muncke, C., Parton, R.G., Kloog, Y., Henis, Y.I., and Hancock, J.F. (2004). Three separable domains regulate GTP-dependent association of H-ras with the plasma membrane. Mol. Cell. Biol. *24*, 6799–6810.

Seabra, M.C., Reiss, Y., Casey, P.J., Brown, M.S., and Goldstein, J.L. (1991). Protein farnesyltransferase and geranylgeranyltransferase share a common alpha subunit. Cell *65*, 429–434.

Sebti, S.M., and Hamilton, A.D. (2000). Farnesyltransferase and geranylgeranyltransferase I inhibitors and cancer therapy: lessons from mechanism and bench-to-bedside translational studies. Oncogene *19*, 6584–6593.

Stenmark, H. (2009). Rab GTPases as coordinators of vesicle traffic. Nat. Rev. Mol. Cell Biol. *10*, 513–525.

Stenmark, H., Parton, R.G., Steele-Mortimer, O., Lütcke, A., Gruenberg, J., and Zerial, M. (1994). Inhibition of rab5 GTPase activity stimulates membrane fusion in endocytosis. EMBO J. *13*, 1287–1296.

Tian, T., Harding, A., Inder, K., Plowman, S., Parton, R.G., and Hancock, J.F. (2007). Plasma membrane nanoswitches generate high-fidelity Ras signal transduction. Nat. Cell Biol. *9*, 905–914.

Vasudevan, A., Qian, Y., Vogt, A., Blaskovich, M.A., Ohkanda, J., Sebti, S.M., and Hamilton, A.D. (1999). Potent, highly selective, and non-thiol inhibitors of protein geranylgeranyltransferase-I. J. Med. Chem. *42*, 1333–1340.

Vogel, S.S., Thaler, C., and Koushik, S.V. (2006). Fanciful FRET. Sci. STKE *2006*, re2.

Voice, J.K., Klemke, R.L., Le, A., and Jackson, J.H. (1999). Four human ras homologs differ in their abilities to activate Raf-1, induce transformation, and stimulate cell motility. J. Biol. Chem. *274*, 17164–17170.

Webb, Y., Hermida-Matsumoto, L., and Resh, M.D. (2000). Inhibition of protein palmitoylation, raft localization, and T cell signaling by 2-bromopalmitate and polyunsaturated fatty acids. J. Biol. Chem. *275*, 261–270.

Yan, J., Roy, S., Apolloni, A., Lane, A., and Hancock, J.F. (1998). Ras isoforms vary in their ability to activate Raf-1 and phosphoinositide 3-kinase. J. Biol. Chem. *273*, 24052–24056.

Zacharias, D.A., Violin, J.D., Newton, A.C., and Tsien, R.Y. (2002). Partitioning of lipid-modified monomeric GFPs into membrane microdomains of live cells. Science *296*, 913–916.

Zerial, M., and McBride, H. (2001). Rab proteins as membrane organizers. Nat. Rev. Mol. Cell Biol. *2*, 107–117.

Zhang, J.H., Chung, T.D., and Oldenburg, K.R. (1999). A simple statistical parameter for use in evaluation and validation of high throughput screening assays. J. Biomol. Screen. *4*, 67–73.

